

PAPER • OPEN ACCESS

WS₂ and MoS₂ thin film gas sensors with high response to NH₃ in air at low temperature

To cite this article: Topias Järvinen *et al* 2019 *Nanotechnology* **30** 405501

View the [article online](#) for updates and enhancements.



IOP | ebooks™

Bringing you innovative digital publishing with leading voices to create your essential collection of books in STEM research.

Start exploring the collection - download the first chapter of every title for free.

WS₂ and MoS₂ thin film gas sensors with high response to NH₃ in air at low temperature

Topias Järvinen¹, Gabriela S Lorite¹, Jani Peräntie¹, Geza Toth²,
Simo Saarakkala³, Vesa K Virtanen³  and Krisztian Kordas^{1,4} 

¹Microelectronics Research Unit, Faculty of Information Technology and Electrical Engineering, University of Oulu, PO Box 4500, FI-90014 University of Oulu, Finland

²VTT Technical Research Center of Finland, PO Box 1100, FI-90571, Oulu, Finland

³Research Unit of Medical Imaging, Physics and Technology, Faculty of Medicine, University of Oulu, PO Box 5000, FI-90014 University of Oulu, Finland

E-mail: krisztian.kordas@oulu.fi

Received 16 April 2019, revised 12 June 2019

Accepted for publication 27 June 2019

Published 18 July 2019



CrossMark

Abstract

Transition metal dichalcogenides (TMDs) have received immense research interest in particular for their outstanding electrochemical and optoelectrical properties. Lately, chemical gas sensor applications of TMDs have been recognized as well owing to the low operating temperatures of devices, which is a great advantage over conventional metal oxide based sensors. In this work, we elaborate on the gas sensing properties of WS₂ and MoS₂ thin films made by simple and straightforward thermal sulfurization of sputter deposited metal films on silicon chips. The sensor response to H₂, H₂S, CO and NH₃ analytes in air at 30 °C has been assessed and both MoS₂ and WS₂ were found to have an excellent selectivity to NH₃ with a particularly high sensitivity of $0.10 \pm 0.02 \text{ ppm}^{-1}$ at sub-ppm concentrations in the case of WS₂. The sensing behavior is explained on the bases of gas adsorption energies as well as carrier (hole) localization induced by the surface adsorbed moieties having reductive nature.

Supplementary material for this article is available [online](#)

Keywords: 2D materials, gas sensors, WS₂, MoS₂, room temperature sensing, NH₃

(Some figures may appear in colour only in the online journal)

Introduction

Continuous and reliable detection of different gases is essential in industrial process monitoring, vehicle emission control, in and outdoor air quality safety and environment protection [1]. In these applications, traditionally metal oxide semiconductors such as SnO₂, WO₃, CeO₂, Nb₂O₅ and ZnO

as well as their metal or metal oxide decorated derivatives have been most commonly utilized as sensing materials [2–5]. While these sensors and their arrays offer excellent and reliable discrimination and even quantification of analytes, their operation is only possible at high temperatures that requires considerable power sourcing. Nowadays, with the spread of internet-of-things and dispersed networks that involve complex sensing systems with small but large number of devices, power consumption becomes a significant factor. Powering such devices is even more cumbersome in the case of remote and autonomous off-grid systems [6–8] running on batteries and/or energy scavenging units with limited power output [9]. Accordingly, new materials that would allow for low temperature operation could inevitably alleviate power related

⁴ Author to whom any correspondence should be addressed.



Original content from this work may be used under the terms of the [Creative Commons Attribution 3.0 licence](#). Any further distribution of this work must maintain attribution to the author(s) and the title of the work, journal citation and DOI.

challenges and contribute to better and more robust sensor networks.

2D layered transition metal dichalcogenides (TMDs) have recently been found very attractive for a wide range of applications such as energy storage, photodetectors and switches, electrocatalysis, photocatalysis as well as for chemoresistive sensors [10–14]. TMDs (MX_2 , where M is a transition metal and X is a chalcogen) have a layered structure, in which the coordination of metal atoms can be trigonal or octahedral resulting in either hexagonal or rhombohedral structure symmetry [15–17]. These materials have not only high specific surface area but as the covalent layers are held together with weak van der Waals forces, and thus have large interplanar spacing, intercalation of small moieties in between the layers is also possible making such structures suitable for multitude interactions with the environment. Recent studies of WS_2 and MoS_2 as well as their hybrid structures (functionalized nanofibers [18, 19], quantum dots [20] and metal doped nanoflower structures [21]) in gas sensing applications indicate substantial response at low operating temperatures with particular selectivity to certain gases such as H_2S and NH_3 [18, 22–24]. The lowered operation temperature of transition metal chalcogenide-based sensors, in reference to the oxides of the corresponding metals, is due to their typically lower bandgap and better conductivity. Furthermore, similar to semiconducting metal oxide sensors, the gas selectivity of TMDs is in many instances associated to the affinities of surfaces for adsorbing different analytes and related surface charging/polarization effects [18, 24]. In addition, it has been identified that apart from surface charging/polarization, reversible doping of the chalcogenide lattice with heteroatoms can significantly contribute to sensing [18].

The aim of the present work is to elaborate on the low temperature gas sensing properties of TMDs produced by sulfurizing sputter deposited tungsten and molybdenum films. As we show, the direct synthesis of WS_2 and MoS_2 thin films on Si chips is robust and offer a route which is up and down-scalable without necessitating any transfer steps of 2D materials [24]. Thin films of crystalline WS_2 grown on Si chips display distinct selectivity towards NH_3 with a sensitivity of $0.10 \pm 0.02 \text{ ppm}^{-1}$, even at 30°C . Interestingly, the surfaces remain practically irresponsive to other analytes (CO , H_2 , and H_2S), which is unexpected in the light of our previous studies on WS_2 nanowire-nanoflake hybrids that showed unprecedented selectivity and sensitivity to H_2S .

Experimental

Materials and sensor fabrication

A $4''$ p-type Si wafer with 1500 nm thermal oxide layer was pre-cut to $7 \times 7 \text{ mm}^2$ size chips using a pulsed laser (LPKF ProtoLaser U3). The chips were then coated with metal films (W or Mo) of 20 nm thickness by sputtering (Torr International PVD System) and sulfurized subsequently. The sulfurization was carried out in a tube furnace (Thermo Scientific Thermolyne having a quartz tube of $2''$ in diameter) in which

four identical chips at a time were inserted together with 1.0 g of sulfur powder (Sigma-Aldrich 215236). Before heating up the furnace, the reactor was evacuated to a base pressure of about 5 Torr and purged with N_2 . After repeating the pumping and purging steps three times, the reactor was heated to 800°C and a flow of 400 sccm N_2 was set and maintained throughout the process. (Note: experiments using Ti and Cr metal thin films were also carried out but as turned out, the sulfurized films were not electrically conductive.)

Contact electrodes were deposited on the chips by sputtering films of Ti (25 nm) and then Pt (220 nm) through a shadow mask (laser patterned polycrystalline alumina with a thickness of $250 \mu\text{m}$) mounted on the chips. The mask pattern was designed to house two pairs of electrodes, each with a gap of $500 \mu\text{m}$.

Materials characterization

Atomic force microscopy (AFM, MultiMode 8, Nanoscope V, Bruker) was used to evaluate the surface topology and root mean square roughness of the sulfurized films using conical Si probes (NSC18/Al BS MikroMash, Tallin, Estonia) in PeakForce mode. Each film was scanned over $10 \times 10 \mu\text{m}^2$ and $1 \times 1 \mu\text{m}^2$ areas. All AFM images were processed and analyzed using Gwyddion software. Particle size distribution curves were compiled by counting at least 150 particles of each film in the AFM topology maps.

The chemical composition and crystal structure of the sulfurized films were characterized using energy-dispersive x-ray spectroscopy (EDS, Zeiss ULTRA Plus with multiple point analysis and averaging), Raman spectroscopy (Thermo Scientific DXR2xi Raman imaging microscope, 532 nm wavelength and 10 mW power) and grazing incidence x-ray diffraction (GIXRD, Bruker D8 Discovery, Cu K_α , 2θ sweep from 10° to 80° at a fixed grazing incidence angle of 4.5°).

Electrical and gas sensing measurements

The conductance of the films was assessed with current–voltage (I – V) measurements by probing the Ti/Pt contact electrode pads with a Wentworth Labs probe station connected to a Keithley 2636A SYSTEM SourceMeter[®]. Voltage sweeps between -5 and 6 V were applied in each measurement. Because of the poor conductivity of sulfurized Ti and Cr, only the MoS_2 and WS_2 films were considered for further analyses.

Gas sensitivity measurements were performed in a temperature controlled chamber (Linkam TMS 94) connected to mass flow controllers (MKS Instruments 1179A Mass-Flo[®]). The analyte gases we used were H_2 (AGA, 99% N_2 , 1% H_2), CO (AGA, 50 ppm CO in N_2), NH_3 (AGA, 50 ppm NH_3 in N_2), and H_2S (AGA, 200 ppm H_2S in N_2), all buffered in synthetic air (AGA, 80% N_2 , 20% O_2) at total flow rates from 500 sccm to 1000 sccm (depending on the analyte gas and its desired concentration range). The measurement profile had a 60 min stabilizing period in the beginning, which was followed by analyte pulses of 30 min duration with increasing concentrations. Between each pulse,

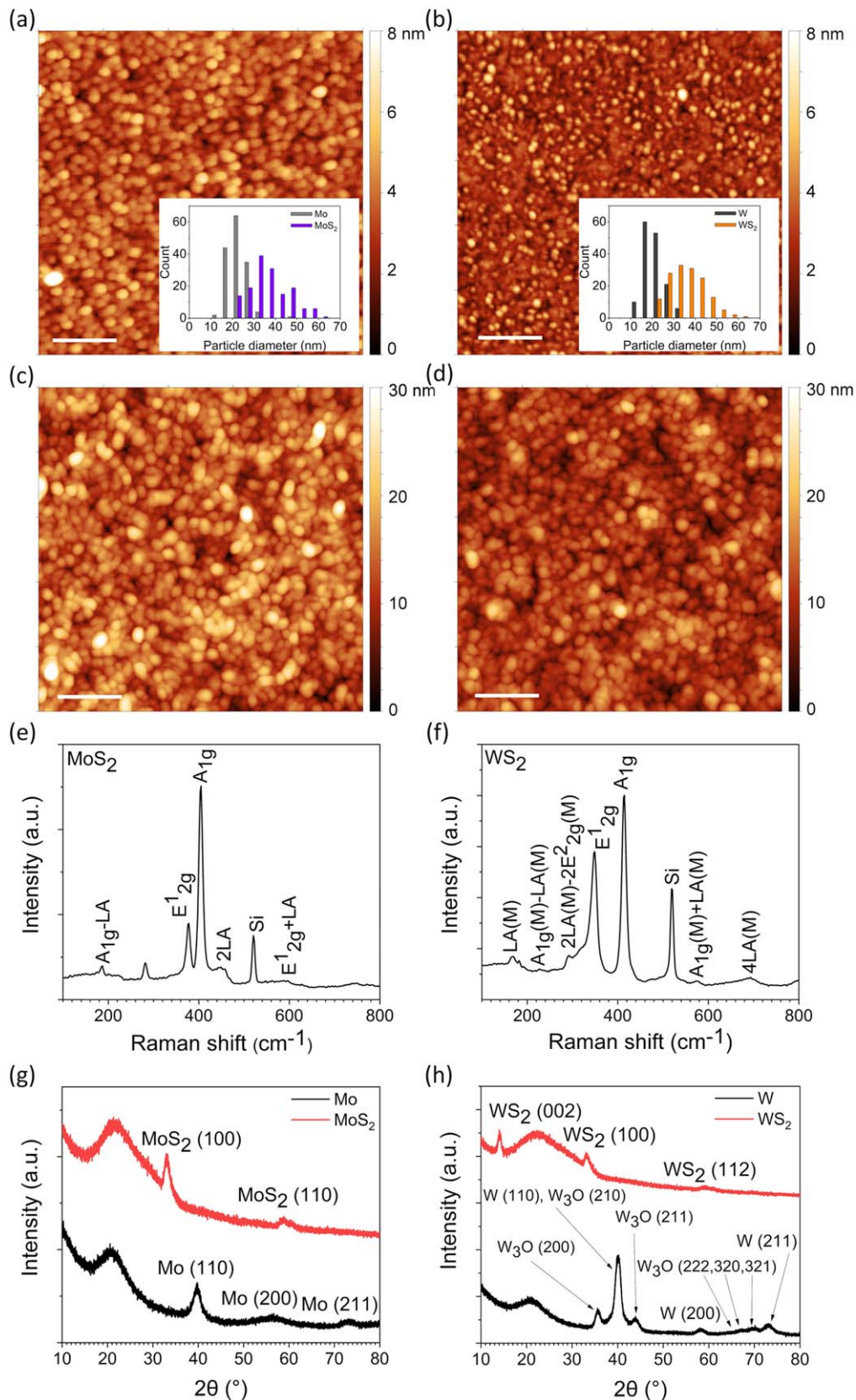


Figure 1. AFM surface topologies of sputter deposited (a) Mo and (b) W thin films as well as their sulfurized derivatives displayed in panels (c) and (d), respectively. Scale bars indicate 200 nm. Insets show the evolution of particle size in the films before and after sulfurization. Raman spectra of sulfurized (e) Mo and (f) W confirming the corresponding phases in the thin films are MoS₂ and WS₂. Panels (g) and (h) are the respective x-ray diffraction patterns acquired using grazing incidence setup including the original and sulfurized W and Mo films.

Table 1. EDS elemental compositions (in at%) averaged for four points of each material.

	C	O	Si	S	W	Mo	M:S ratio
MoS ₂	0	44.5	48.1	5.3	0	2.1	1:2.5
WS ₂	23.5	32.4	35.9	5.4	2.7	0	1:2.0

a 30 min long recovery period was applied. The temperature of the gas chamber was kept constant at 30 °C. Gas responses of the devices were measured with a multimeter (Hewlett-Packard 3458 A) at constant bias of 1 V in 10 s sampling intervals, and logged with LabVIEW™ (National Instruments). In total, six samples were measured for each MoS₂ and WS₂ based devices. The measurement data was imported to Origin® 2018b (OriginLab Corporation) and processed further to compensate for the baseline drift.

Results and discussion

AFM images of large scans areas (10 × 10 μm²) revealed the sulfurized Mo films were uniform, whereas the sulfurized W layers had some small pinholes of 0.5–2 μm in diameter (not shown here). Apart from the surface defects in the sulfurized W layer, both products were found homogeneous with grain-like morphology. The original particle size of the metal films increased from 23 ± 4 nm (Mo) and 21 ± 4 nm (W) to 37 ± 9 nm and 36 ± 8 nm, respectively. The particle size distributions (inset panels) seem to follow a log-normal curve rather than Gaussian. The increased particle diameters are likely caused by the formation of the corresponding sulfides, having lower density than that of the corresponding metals (figures 1(a)–(d)).

Raman spectra of the films displayed in figures 1(e) and (f) indicate the materials are crystalline MoS₂ and WS₂, respectively [25, 26]. Two strong peaks are observed for MoS₂ at 378 and 405 cm⁻¹ that correspond to the in-plane (E_{2g}¹) and out-of-plane (A_{1g}) vibration modes [27]. According to the difference of Raman shifts and also to the intensity ratio of these two peaks, MoS₂ is multi-layered [28]. Likewise, the WS₂ film has two intensive peaks at 349 and 415 cm⁻¹ that can be assigned to in-plane (E_{2g}¹) and out-of-plane (A_{1g}) vibration modes, evidencing that the structure is multi-layered [29, 30]. The presence of the longitudinal acoustic mode vibrations (LA) and their higher-order harmonics (2LA and 4LA) are also visible in the spectra. The low intensity of the 2LA peaks confirms the chalcogenides are multi-layered [26]. Note, that in each spectrum, the relatively intensive peak at around 520 cm⁻¹ is due to the Si substrate.

Grazing incidence x-ray diffraction patterns of the original and sulfurized metal films are displayed in figures 1(g) and (h). The metal films pattern fits well the reference patterns PDF 42-1120 and PDF 01-1204 for Mo and W, respectively. In addition, the metallic tungsten film shows some W₃O which is indexed according to PDF 02-1138. The pattern of MoS₂ shows two strong reflections at 33.2° and 59.5°, which may be indexed as the (100) plane and superposed reflections

from the (110) and (008) planes of the hexagonal form of the crystal (PDF 75-1539). However, the strong reflections of the (002) and (102) planes at 14.1° and 36.0° of layered structure that should be also present in the pattern are missing from our diffractogram suggesting the lack of long-range order in stacking of the layers in the material. Another explanation might be a specific crystal orientation on the substrate with basal planes being perpendicular to the surface. However, this latter option is unlikely, since the AFM images show spherical particles on the surfaces that do not resemble oriented crystals. On the other hand, in the case of the WS₂ film, the pattern can be assigned to the planes of the hexagonal lattice (PDF 02-0131). The reflection at 14.1° corresponds to the (002) plane, the broad peak at 33.1° is due to the superposed intensities of the (100) and (101), whereas the broad reflection centered at 59.0° can be assigned to the unresolved (110), (008) and (112) planes [29]. It is also worth noting here, that the broad reflection at around 20.0° is due to amorphous SiO₂ of the substrate.

The composition of the films was analyzed with EDS (table 1). The aforementioned pinhole defects seen in WS₂ films comprise only silicon and oxygen confirming that the defects are indeed voids in the film. Since the thickness of TMD films is ~20 nm, both Si and O of the Si/SiO₂ substrate are visible in the energy-dispersive x-ray spectra even at locations without pinholes. The ratio of sulfur and metal is very close to 2:1 for both TMD films, which implies the films are at least nearly stoichiometric. In the case of WS₂ there is a notable amount of C contamination present, which was not observed in MoS₂ films.

Before the actual sensor measurements, the electrical conductivity of each film was assessed with *I*–*V* measurements. Both MoS₂ and WS₂ films were sufficiently conductive (with resistances of several tens of megaohms and hundreds of megaohms, respectively) to perform sensor measurements on those. The *I*–*V* curves were found linear for MoS₂, whereas WS₂ showed slight nonlinearity (figures 2(a) and (d), respectively), suggesting a barrier between the semiconducting film and the Ti/Pt electrodes [31]. Although the primary direct contact with the chalcogenide films was meant to be Ti, some Pt also deposited on the films around the perimeter of the Ti under-metallization due to the imperfect contact between the shadow mask and the substrate. Considering the typical bandgap, electron affinity and the work function values of bulk MoS₂ (E_g ~ 1.3 eV, χ ~ 4.0 eV and φ ~ 5.25 eV)[32, 33] and WS₂ (1.4, 4.0 and 5.1 eV) [34] as well as the work function values of Ti (φ_{Ti} ~ 4.3 eV) and Pt (φ_{Pt} ~ 5.3 eV), we find that the contact between Ti and the chalcogenide films is Schottky-type (figures 2(b) and (e)), whereas it is quasi-ohmic with Pt (figures 2(c) and (f)). Furthermore, because of the better alignment of the Fermi level of Pt with the valence band of MoS₂ in reference to WS₂, the ohmic character is also expected to be better, which explains the good linearity of the *I*–*V* slopes and higher conductivity for the MoS₂ based devices and slight nonlinearity measured for the WS₂ based ones.

In general, WS₂ based devices were electrically less conductive but had considerably higher response to the

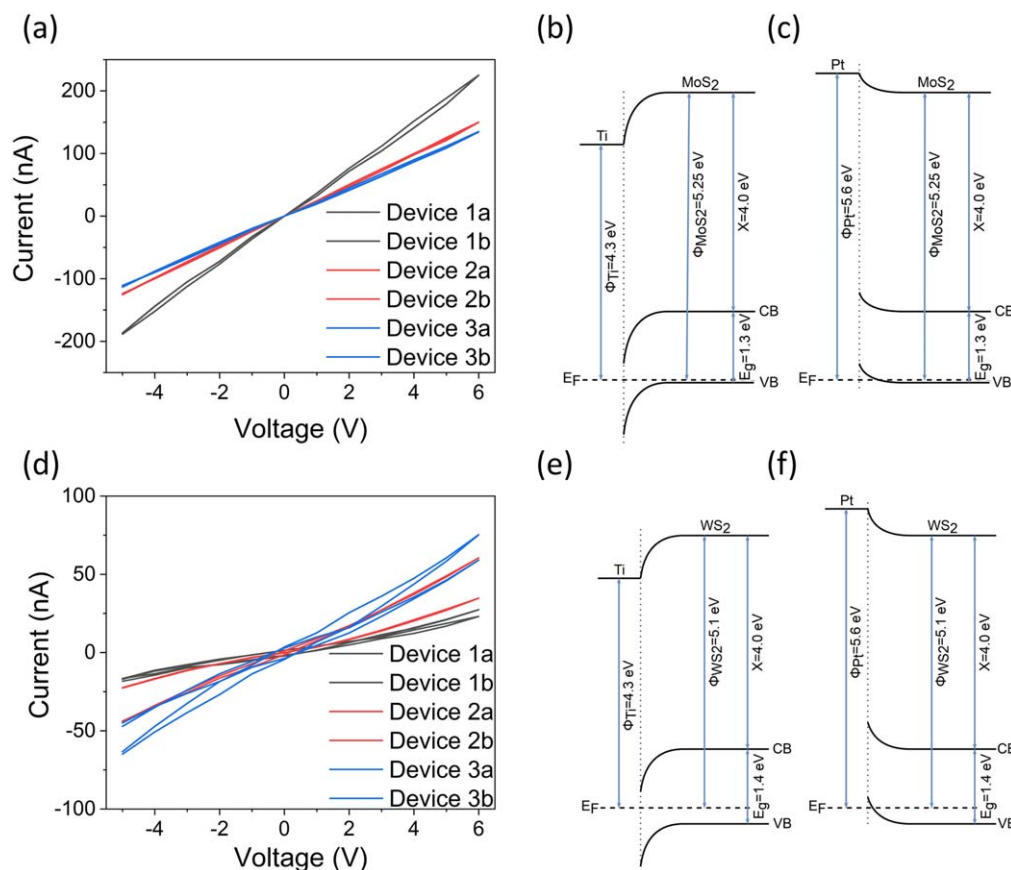


Figure 2. *IV* curves of (a) MoS₂ and (d) WS₂. Three sensor devices with two pairs of electrodes, totaling six samples, were measured for each material. The metal–semiconductor junctions for the films and contact electrodes of titanium and platinum are presented in (b), (c) for MoS₂ and (e), (f) for WS₂, respectively. Note: the energy values used for depicting the band diagrams may not be entirely accurate, as each value shows variation depending on the structure and method of determination, as shown in table S1, available online at stacks.iop.org/NANO/30/405501/mmedia in the supplementary information.

analytes, although with higher device-to-device variation (average of six devices for each gas) in reference to MoS₂ sensors (figures 3 and 4(c)). The films show a small response to H₂ ($0.00005 \pm 0.00003 \text{ ppm}^{-1}$ and $0.00016 \pm 0.00017 \text{ ppm}^{-1}$ for MoS₂ and WS₂, respectively). This is comparable to previous results with WS₂ nanowire/nanoflake hybrid structures [18]. For H₂S and CO the responses were either nonexistent or inconsistent. Regardless of the variance of the response to other analytes, for NH₃ the devices display a consistent and very good response ($0.0026 \pm 0.0022 \text{ ppm}^{-1}$ and $0.0586 \pm 0.0305 \text{ ppm}^{-1}$ for MoS₂ and WS₂, respectively).

Since the response to NH₃ with both sensors was very distinct at 1 ppm gas concentration, additional measurements were performed in the sub-ppm NH₃ concentrations. Significant responses to 200 ppb of the analyte could be measured with average sensitivities of $0.0315 \pm 0.00282 \text{ ppm}^{-1}$ and $0.104 \pm 0.0243 \text{ ppm}^{-1}$, respectively (figure 4). According to the signal to the base noise ratio, the limit of detection (LOD) is under 100 ppb for both materials. The response time of the MoS₂ based sensors to the analytes were found to be rather short for NH₃ (5–6 min) and slightly longer for other gases (10–30 min). The sensor recovery time constants were long (30–60 min) and varied greatly among the gases. On the

other hand, sensors made of the WS₂ films showed a consistent and quick (5–6 min) response and recovery for each gas, which is excellent considering that the measurements were carried out at near room temperature.

According to the reducing nature of all the analyte gases and the response of the sensors, it can be concluded that both WS₂ and MoS₂ exhibit p-type semiconducting behavior, and the resistance of the sensors increase with the concentration of the analytes. This is usually explained by surface adsorption and subsequent charge transfer based mechanisms; the reducing gases donate electrons (or localize holes) in the materials, thus reducing the concentration of charge carriers, and consequently reduce the conductivity of the material [18, 20]. A number of other studies show selectivity to NH₃ for both WS₂ [22, 23, 31, 35] and MoS₂ [20, 36, 37]. In the case of MoS₂, the LOD of 100 ppb is similar to other results (300 ppb measured and 50 ppb predicted) [24]. In the case of WS₂, the reported LODs are about a decade worse ($\sim 1 \text{ ppm}$) [38, 23] than our data. (In table S2, we list a more detailed comparison of the results with other reported values for MoS₂ and WS₂ based devices and commercial NH₃ sensors.)

As the sensing behavior of the thin films presented in the manuscript is similar to or better than those reported for other MX₂ based devices regarding NH₃, we may assume that the

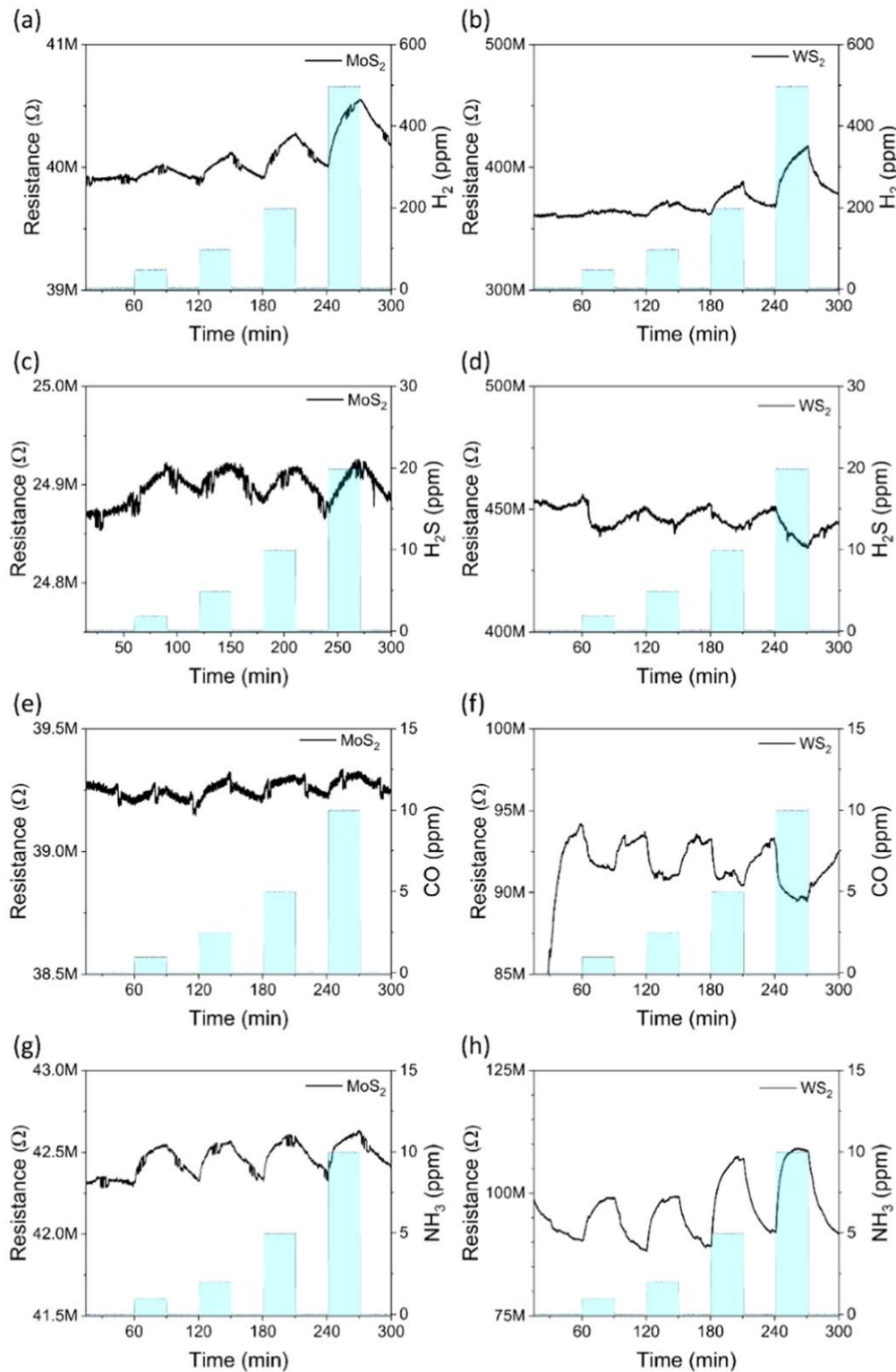


Figure 3. Baseline corrected responses to MoS₂ ((a), (c), (e), (g)) for H₂, H₂S, Co and NH₃ and WS₂ films ((b), (d), (f), (h)), respectively. Note: the responses represent the best performing sample of the material for the particular analyte.

sensing mechanism is also similar, i.e. associated with surface adsorption and consequent partial charge transfer. Calculated (local-density approximation, LDA) surface adsorption energies of H₂, NH₃ and CO on MoS₂ with corresponding values of -82 meV, -250 meV and -128 meV, respectively, also seem to support the high response to NH₃ on MoS₂ films

[20, 39]. Similarly, on WS₂, the calculated energies [18] are -57.4 meV (H₂), -171.7 meV (NH₃), and -84.7 meV (CO) indicating that the response to NH₃ is expected to be the highest. Here, we have to point out another effect regarding H₂S. Namely, considering the high adsorption energy of H₂S (-181 meV) on WS₂ nanosheets, we shall also expect to see

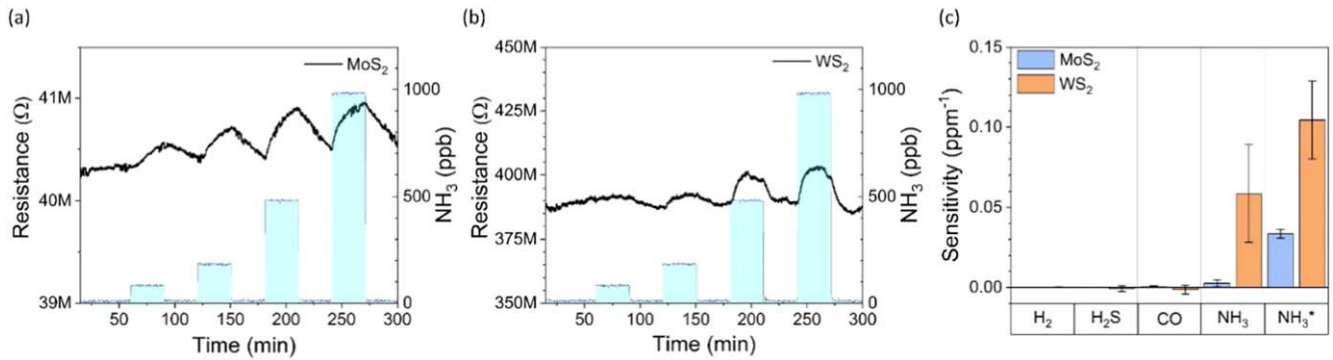


Figure 4. Response of MoS₂ (a) and WS₂ (b) for sub-ppm levels of NH₃. (c) Average sensitivities for each gas calculated for the smallest observable responses measured in the ppm range. Data for NH₃ shows the sensitivity measured at 200 ppb for both MoS₂ and WS₂.

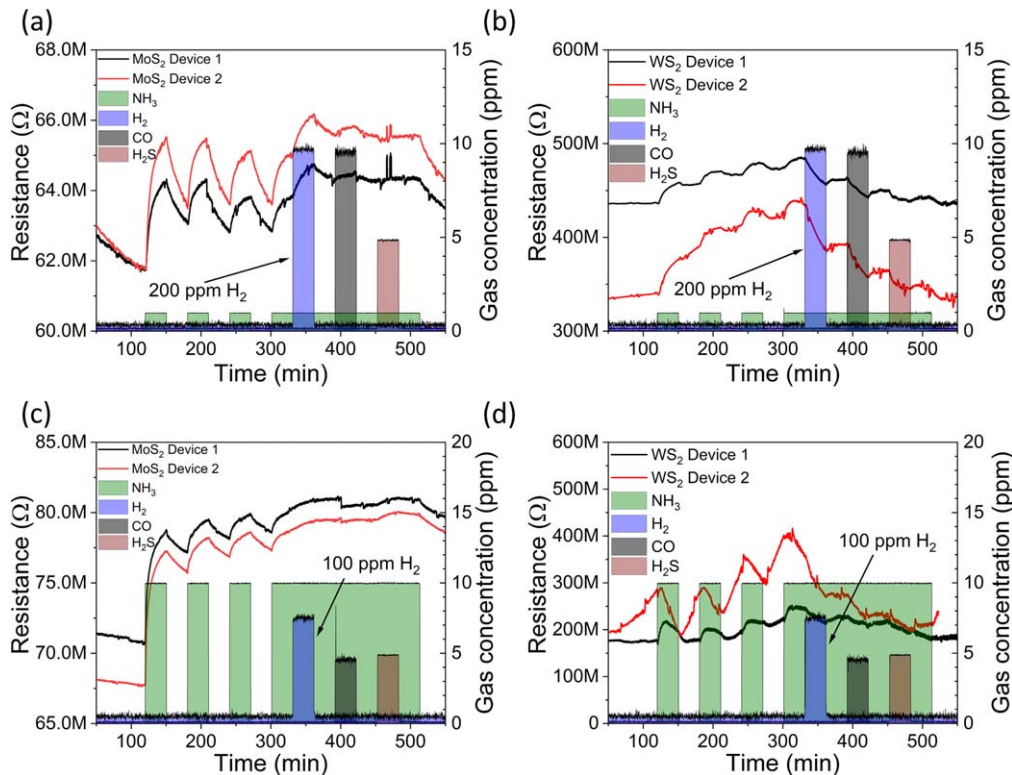


Figure 5. Cross-sensitivity analysis of the sensors using (a), (b) low concentration NH₃, and high concentration H₂, CO and H₂S pulses as well as (c), (d) similar analyte concentrations during the measurements.

good response to H₂S. However, this is not the case with our thin films. The reason is that competitive lattice doping with O and S is responsible for the detection of H₂S as we have concluded in our earlier work [18] based on XPS analysis of WS₂ nanowire-nanoflake hybrid structures, in which nanosheets of ~5 nm thickness were sticking out from the surface of the nanowires. The structure is different now, since both WS₂ and MoS₂ films are comprising nanoparticles of 20–30 nm in their diameter with limited diffusion of O and S in the lattices, thus despite the large adsorption energy of H₂S, the sensor response is insignificant to this analyte.

To analyze the cross-sensitivity of the sensors, we performed two sets of measurements for two samples of each material (figure 5). In the first set, we applied gas pulses with concentrations of 1 ppm, 200 ppm, 10 ppm and 5 ppm for

NH₃, H₂, CO and H₂S, respectively. In the other set, the respective concentrations were 10, 100, 5 and 5 ppm. The sensitivity to NH₃ remained high for all samples throughout the measurements (the first three pulses in each plot), which proves the repeatability and reproducibility of the devices. During the long 4th pulse of NH₃ (starting at 300 min) we introduced also H₂, then CO and H₂S for short intervals (30 min each starting at 330 min, 390 min and 460 min, respectively) to see the influence of the secondary analytes. The MoS₂ film was affected only by H₂ but only when its concentration was high relative to the concentration of NH₃ (figure 5(a)). The influence of secondary analytes on the response to NH₃ introduced at similar concentrations was insignificant (figure 5(c)). However, in the case of the WS₂ based device, we observe a decreased response to low

concentration NH_3 , when introducing the other gases at high concentrations (figure 5(b)). The effect is lower, when the analyte concentrations were adjusted to be similar (figure 5(d)). The results measured with WS_2 sensors indicate, that the secondary gas pulses can flush away the surface adsorbed NH_3 thus influencing the sensor performance.

Furthermore, it is worth pointing out that all sensors were operating in a rather reliable and repeatable manner throughout a period of more than nine month testing in various experimental conditions, which indicates that the thin film WS_2 and MoS_2 structures are very robust and practical.

Conclusions

A method to produce MoS_2 and WS_2 thin films by simply annealing sputtered Mo and W films in S vapor is proposed, and the gas response of the as-synthesized films are examined in the classical resistive sensor arrangement. Both materials showed excellent selectivity for NH_3 with very high corresponding sensitivity values ($0.03 \pm 0.0 \text{ ppm}^{-1}$ and $0.10 \pm 0.02 \text{ ppm}^{-1}$, respectively) at 30°C . Despite the low operation temperature, the WS_2 based sensors responded to the stimuli and then recovered after each gas pulse quite fast (5–6 min). The results obtained with our robust TMD films compete with other exfoliated or CVD grown single or few-layer chalcogenides and outperforms metal oxides. Since the process steps involved apply standard techniques, up and down-scalable, and the films produced are easy to process further (e.g. coating with other materials) the results presented in this paper may pave the road for sensor applications of TMD thin films.

Acknowledgments

Support received from the Väisälä Foundation, Riitta and Jorma J. Takanen Foundation, Academy of Finland (298409), University of Oulu (Project: Entity) and European Union Interreg Nord – Lapin liitto (Project: Transparent, conducting and flexible films for electrodes) are acknowledged. Kai Metsäkoivu (Center of Microscopy and Nanotechnology, University of Oulu) is acknowledged for the metal films deposition.

Conflicts of interest

The authors declare no conflicts interest.

ORCID iDs

Vesa K Virtanen  <https://orcid.org/0000-0002-5797-5365>

Krisztian Kordas  <https://orcid.org/0000-0002-7331-1278>

References

- [1] Meixner H and Lampe U 1996 Metal oxide sensors *Sensors Actuators B* **33** 198–202
- [2] Neri G 2015 First fifty years of chemoresistive gas sensors *Chemosensors* **3** 1–20
- [3] Kukkola J et al 2012 Inkjet-printed gas sensors: metal decorated WO_3 nanoparticles and their gas sensing properties *J. Mater. Chem.* **22** 17878
- [4] Kukkola J, Mohl M, Leino A-R, Mäklän J, Halonen N, Shchukarev A, Konya Z, Jantunen H and Kordas K 2013 Room temperature hydrogen sensors based on metal decorated WO_3 nanowires *Sensors Actuators B* **186** 90–5
- [5] Dey A 2018 Semiconductor metal oxide gas sensors: a review *Mater. Sci. Eng. B* **229** 206–17
- [6] Aponte-Luis J et al 2018 An efficient wireless sensor network for industrial monitoring and control *Sensors* **18** 182
- [7] Somov A, Baranov A, Savkin A, Spirjakin D, Spirjakin A and Passerone R 2011 Development of wireless sensor network for combustible gas monitoring *Sensors Actuators* **171** 398–405
- [8] Jarvinen T, Lorite G S, Rautio A-R, Koppany L J, Kukovec A, Konya Z, Kordas K and Toth G 2017 Portable cyber-physical system for indoor and outdoor gas sensing *Sensors Actuators B* **252** 983–90
- [9] Akhtar F and Rehmani M H 2015 Energy replenishment using renewable and traditional energy resources for sustainable wireless sensor networks: a review *Renew. Sustain. Energy Rev.* **45** 769–84
- [10] Kuc A 2014 Low-dimensional transition-metal dichalcogenides *Chemical Modelling* vol 11 (London: Royal Society of Chemistry) pp 1–29
- [11] Li B L, Wang J, Zou H L, Garaj S, Lim C T, Xie J, Li N B and Leong D T 2016 Low-dimensional transition metal dichalcogenide nanostructures based sensors *Adv. Funct. Mater.* **26** 7034–56
- [12] Kim T, Kim Y, Park S, Kim S, Jang H, Kim T H, Kim Y H, Park S Y, Kim S Y and Jang H W 2017 Two-dimensional transition metal disulfides for chemoresistive gas sensing: perspective and challenges *Chemosensors* **5** 15
- [13] Eftekhari A 2017 Tungsten dichalcogenides (WS_2 , WSe_2 , and WTe_2): materials chemistry and applications *J. Mater. Chem. A* **5** 18299–325
- [14] Hasani A, Tekalgne M, Van L Q, Jang H W and Kim S Y 2019 Two-dimensional materials as catalysts for solar fuels: hydrogen evolution reaction and CO_2 reduction *J. Mater. Chem. A* **7** 430–54
- [15] Andoshe D M, Jeon J-M, Kim S Y and Jang H W 2015 Two-dimensional transition metal dichalcogenide nanomaterials for solar water splitting *Electron. Mater. Lett.* **11** 323–35
- [16] Song I, Park C and Choi H C 2015 Synthesis and properties of molybdenum disulfide: from bulk to atomic layers *RSC Adv.* **5** 7495–514
- [17] Wang Q H, Kalantar-Zadeh K, Kis A, Coleman J N and Strano M S 2012 Electronics and optoelectronics of two-dimensional transition metal dichalcogenides *Nat. Nanotechnol.* **7** 699–712
- [18] Asres G A et al 2018 Ultrasensitive H_2S gas sensors based on p-type WS_2 hybrid materials *Nano Res.* **11** 4215–24
- [19] Cha J-H, Choi S-J, Yu S and Kim I-D 2017 2D WS_2 -edge functionalized multi-channel carbon nanofibers: effect of WS_2 edge-abundant structure on room temperature NO_2 sensing *J. Mater. Chem. A* **5** 8725–32
- [20] Yue N, Weicheng J, Rongguo W, Guomin D and Yifan H 2016 Hybrid nanostructures combining graphene– MoS_2 quantum dots for gas sensing *J. Mater. Chem. A* **4** 8198–203
- [21] Zhang D, Wu J, Li P and Cao Y 2017 Room-temperature SO_2 gas-sensing properties based on a metal-doped MoS_2

- nanoflower: an experimental and density functional theory investigation *J. Mater. Chem. A* **5** 20666–77
- [22] Li X, Li X, Li Z, Wang J and Zhang J 2017 WS₂ nanoflakes based selective ammonia sensors at room temperature *Sensors Actuators B* **240** 273–7
- [23] O'Brien M, Lee K, Morrish R, Berner N C, McEvoy N, Wolden C A and Duesberg G S 2014 Plasma assisted synthesis of WS₂ for gas sensing applications *Chem. Phys. Lett.* **615** 6–10
- [24] Lee K, Gatensby R, McEvoy N, Hallam T and Duesberg G S 2013 High-performance sensors based on molybdenum disulfide thin films *Adv. Mater.* **25** 6699–702
- [25] Gołasa K, Grzeszczyk M, Bożek R, Leszczyński P, Wyszmołek A, Potemski M and Babiński A 2014 Resonant Raman scattering in MoS₂—from bulk to monolayer *Solid State Commun.* **197** 53–6
- [26] Berkdemir A *et al* 2013 Identification of individual and few layers of WS₂ using raman spectroscopy *Sci. Rep.* **3** 1755
- [27] Cwik S, Mitoraj D, Mendoza Reyes O, Rogalla D, Peeters D, Kim J, Schütz H M, Bock C, Beranek R and Devi A 2018 Direct growth of MoS₂ and WS₂ layers by metal organic chemical vapor deposition *Adv. Mater. Interfaces* **5** 1800140
- [28] Li S-L, Miyazaki H, Song H, Kuramochi H, Nakaharai S and Tsukagoshi K 2012 Quantitative raman spectrum and reliable thickness identification for atomic layers on insulating substrates *ACS Nano* **6** 7381–8
- [29] Asres G A *et al* 2016 A novel WS₂ nanowire-nanoflake hybrid material synthesized from WO₃ nanowires in sulfur vapor *Sci. Rep.* **6** 25610
- [30] Viršek M, Jesih A, Milošević I, Damjanović M and Remškar M 2007 Raman scattering of the MoS₂ and WS₂ single nanotubes *Surf. Sci.* **601** 2868–72
- [31] Huo N, Yang S, Wei Z, Li S-S, Xia J-B and Li J 2015 Photoresponsive and gas sensing field-effect transistors based on multilayer WS₂ nanoflakes *Sci. Rep.* **4** 5209
- [32] Baik S S, Im S and Choi H J 2017 Work function tuning in two-dimensional MoS₂ field-effect-transistors with graphene and titanium source-drain contacts *Sci. Rep.* **7** 45546
- [33] Hao G, Huang Z, Liu Y, Qi X, Ren L, Peng X, Yang L, Wei X and Zhong J 2013 Electrostatic properties of few-layer MoS₂ films *AIP Adv.* **3** 042125
- [34] Asres G A *et al* 2018 High photoresponse of individual WS₂ nanowire-nanoflake hybrid materials *Appl. Phys. Lett.* **112** 233103
- [35] Qin Z, Zeng D, Zhang J, Wu C, Wen Y, Shan B and Xie C 2017 Effect of layer number on recovery rate of WS₂ nanosheets for ammonia detection at room temperature *Appl. Surf. Sci.* **414** 244–50
- [36] Late D J *et al* 2013 Sensing behavior of atomically thin-layered MoS₂ transistors *ACS Nano* **7** 4879–91
- [37] Yao Y, Tolentino L, Yang Z, Song X, Zhang W, Chen Y and Wong C 2013 High-concentration aqueous dispersions of MoS₂ *Adv. Funct. Mater.* **23** 3577–83
- [38] Perrozzi F, Emamjomeh S M, Paolucci V, Taglieri G, Ottaviano L and Cantalini C 2017 Thermal stability of WS₂ flakes and gas sensing properties of WS₂/WO₃ composite to H₂, NH₃ and NO₂ *Sensors Actuators B* **243** 812–22
- [39] Wang X, Yang S, Yue Q, Wu F and Li J 2014 Response of MoS₂ nanosheet field effect transistor under different gas environments and its long wavelength photoresponse characteristics *J. Alloys Compd.* **615** 989–93